Supporting Information

Active targeting of cancer cells by CD44 binding peptide-functionalized oil core-based nanocapsules

A. De Capua[1,2], A. Palladino[3], M. Chino[4], C. Attanasio[1,3,*], A. Lombardi[4], R. Vecchione[1,*], P. A. Netti[1,2,5]

1. Center for Advanced Biomaterials for Health Care@CRIB, Istituto Italiano di Tecnologia, Largo Barsanti e Matteucci 53, Napoli, 80125, Italy
2. Department of Chemical, Materials & Industrial Production Engineering, University of Naples Federico II, Naples 80125, Italy
3. Department of Veterinary Medicine and Animal Productions, University of Naples Federico II, Via F. Delpino 1, 80137 Naples, Italy
4. Department of Chemical Sciences, University of Naples Federico II, Complesso Universitario Monte S. Angelo, via Cintia 45, 80126 Naples, Italy
5. Interdisciplinary Research Center of Biomaterials, CRIB, University Federico II, P. le Tecchio 80, 80125 Naples, Italy

NMR characterization

Table S.1: *^{1}H Chemical shift δ, integral and coupling constant J of biotin hydrazide in 90/10 H_2O/D_2O*

Name	δ	H's	Integral	Class	J's
H c	1.30	2	2.04	m	
H b	1.47	3	3.05	m	
H d	1.59	1	1.09	m	
H a	2.18	2	2.00	t	7.4, 7.4
H h'	2.56	1	1.00	d	12.4
H h	2.80	1	1.00	dd	5.1, 12.4
H e	3.08	1	1.00	m	
H f	4.11	1	1.00	m	
H g	4.28	1	1.00	m	

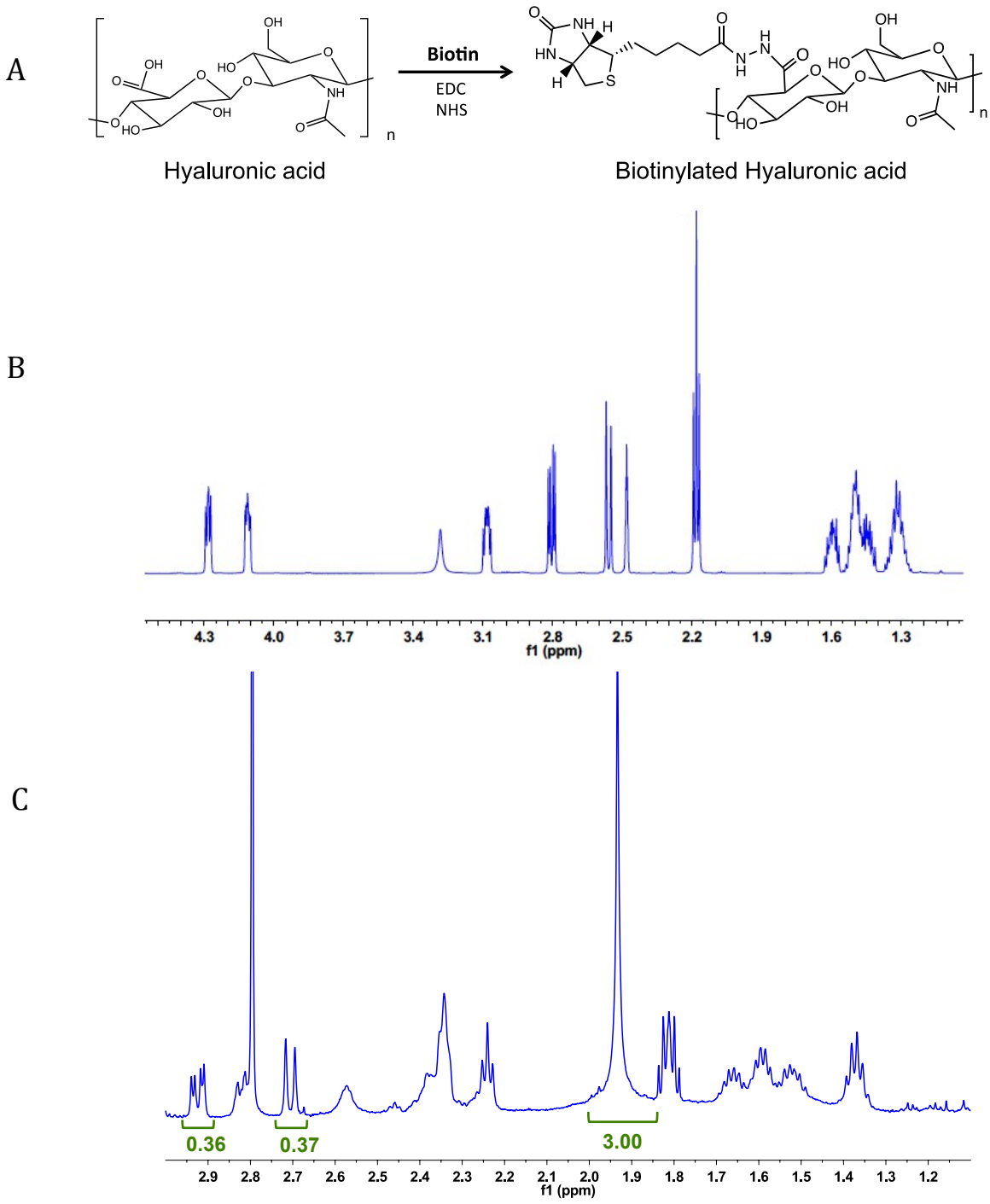

Figure S.1: *(A) Schematic representation of Hyaluronic acid functionalization with biotin. (B) ^{1}H-NMR spectra analysis of biotin hydrazide, (C) ^{1}H-NMR spectra analysis of biotinylated hyaluronic acid in 90/10 H_2O/D_2O. Green lines represent the peak integration.*

^{1}H NMR spectra of biotin hydrazide and biotin-HA were reported in Figure S.1.B, S.1.C. A summary of chemical shift δ assignments, integrals and coupling constant J of biotin-HA spectra is reported in the Table S.2. The peak at chemical shift δ 1.91 ppm was assigned to the acetyl group of HA whereas the doublet at 2.68 ppm and the doublet of doublet at 2.90 ppm was assigned to the protons H *h* and H *h'* of biotin, respectively. The hydrogen H *h* is coupled with the other H *h'* atom and appear as a doublet, while H *h'*, in addition to being coupled to H *h*

(confirmed by the same coupling constant J=13), is also coupled with the proton *g* appearing as doublet of doublet. The peak integration shown in Figure S.1.C was normalized respect to the number of protons of acetyl group, which was assigned to a value of three. The biotin-HA functionalization yield was calculated by the integration of the peaks assigned to biotin protons and to HA acetyl group.

Table S.2: *^{1}H Chemical shift δ, integral and coupling constant J of biotinylated HA in 90/10 H_2O/D_2O.*

Name	δ	Integral	Class	J's
Acetyl group of HA	1.91	3.00	s	
H h of Biotin	2.68	0.37	d	13.00
H h' of Biotin	2.90	0.36	dd	4.93, 13.08

Multilayer deposition of polymers onto O/W NEs

Our research group developed an innovative protocol to deposit a layer of chitosan around the oil template, preserving long-term stability thanks to the implementation of a multi re-dispersion high-pressure process. We also set-up a novel approach to tune the O/W NE dimensions based on the amount of surfactant (lecithin) concentration. A reproducible size control was attained for different formulations, from ~ 160 nm, with the lowest concentration of lecithin (1.9 g, named L_1), to around 90 nm with the highest one (5.8 g, named L_4).[1] Once functionalized with biotin, HA was used to build up a polymer bilayer around the oil core of O/W NE. Firstly, we started using NEs with an intermediate lecithin concentration (L_2, 140 nm) to validate polymer deposition protocol. Saturation method[2] was used to study the optimal concentration ratio between CT and biotinylated HA for the formation of consecutive polyelectrolytes layers, kept together by electrostatic forces, using layer by layer technique[1]. Figure S.2 shows size; PdI and Z-potential data of bilayers coated NEs at different percentage (wt %) of biotinylated HA deposited on the monolayer L_2 0.01 wt % CT-1 wt % O/W NEs.

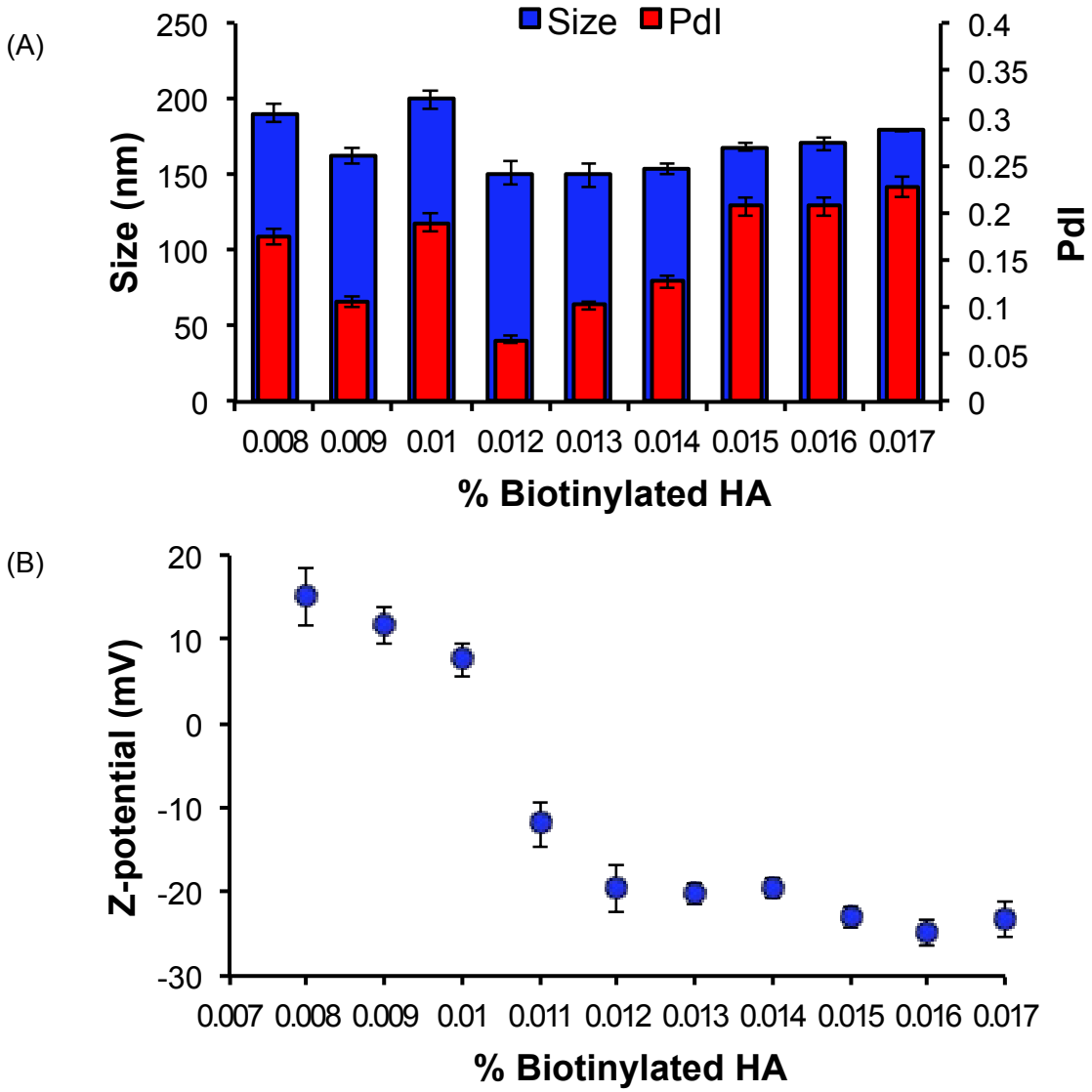

Figure S.2: *DLS Size (A) and Z-Potential (B) data of biotinylated HA at different percentage deposited on monolayer L_2 0.01 wt % CT-1 wt % O/W NEs. Data are reported as mean ± SD (n=3).*

The charge switches from a positive value (+ 15.1 mV) to a negative one, until a plateau is observed, as consequence of the complete biotinylated HA coating above the positive chitosan layer. Dimensional analysis shows that, when the monolayer is not completely covered by HA or an excess of polymer deposition occurs, a destabilization of the system is observed (size around 200 nm and a PdI value that largely exceed the 0.1 value). Therefore, the optimum ratio between HA and CT concentrations (wt %), in term of size (< 160 nm), PdI (< 0.1) and Z-potential (~ -30 mV), is 2.4 (wt %/wt %). A comparison between biotinylated and non-biotinylated multilayer system is shown in Figure S.3. The size of biotinylated and non-biotinylated HA bilayer systems were comparable.

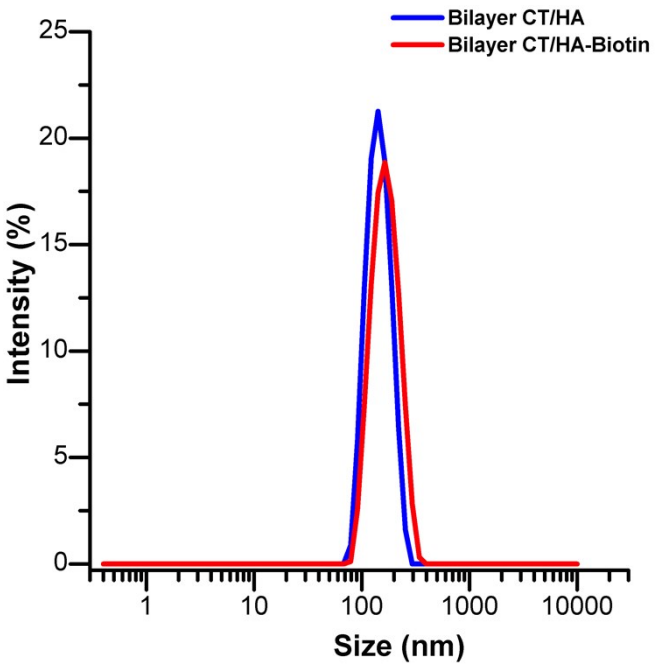

	Size (nm)	PdI	Z-potential (mV)
Bilayer CT-HA	141.2 ± 3.4	0.046 ± 0.004	-21.7 ± 4.5
Bilayer CT-HA-biotin	151 ± 7.9	0.065 ± 0.013	-22.9 ± 1.3

Figure S.3: *Comparison of DLS size and Z-Potential data between bilayer 0.012 wt% HA-biotin-0.005 wt% CT-0.5% O/W NEs and bilayer 0.012 wt% HA-0.005 wt % CT-0.5 % O/W NEs. Data are reported as mean ± SD (n=3).*

Once identified the right conditions, in terms of size stability and Z-potential, to reach the deposition of two polymer layers, we aimed at reducing the dimensions of multi-layers coated O/W NEs. Therefore, we investigated their dimensional behaviour as a result of biotinylated HA depositions above the CT coated O/W NEs formulations made with the smallest nanoemulsion size (L_4). Figure S.4 shows size and Z-potential of the bilayer made with biotinylated HA deposition, at different polymer concentrations, on L_4 0.01 wt % CT-1 wt % O/W NEs. A similar trend was observed, in which, as in the previous case, the optimum ratio between HA and CT concentrations is 2.4 (wt %/wt %). Therefore, the size-scalability of our tool and its narrow distribution was verified. It was demonstrated on two different NEs template (L_2 and L_4), but we would expect the same trend in a wider range of NEs dimensions.

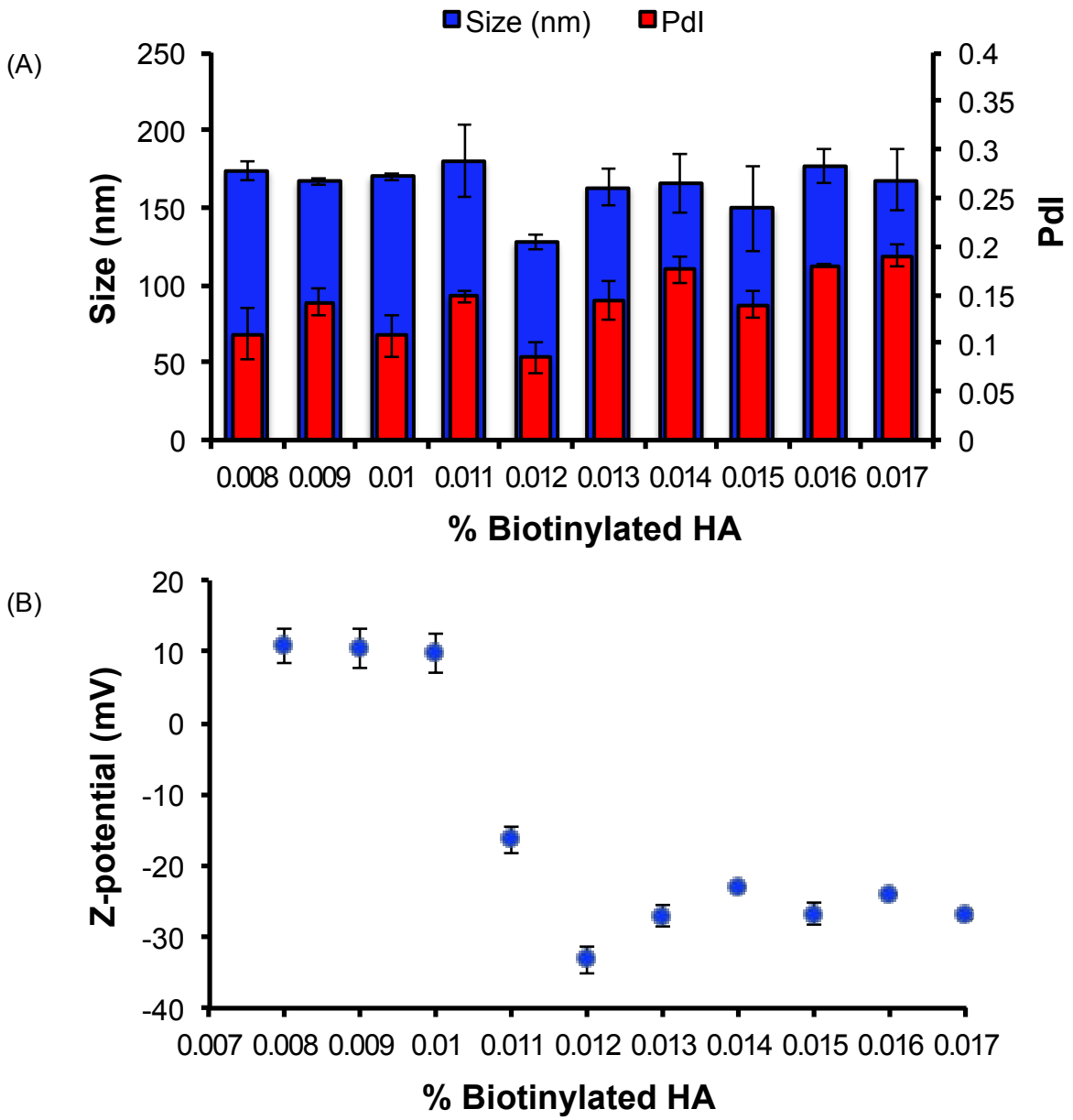

Figure S.4: *(A) DLS Size and (B) Z-Potential data of biotinylated HA at different percentage deposited on monolayer L_4 of 1 wt % oil-chitosan 0.01 wt %. Data are reported as mean ± SD (n=3).*

Isothermal Titration Calorimetry

Table S.3: *Thermodynamic parameters of the interaction between streptavidin and 0.05 wt% HA-biotin-0.02 wt% CT-2.08 wt% O/W NEs at 25 °C.*

Model	Variable	Value
Indipendent	K_d (M)	$8.3\pm0.1 \cdot 10^{-8}$
	*n**	1.8 ± 0.54
	ΔH (kJ/mol)	$-4.4\pm0.3 \cdot 10^{2}$
	TΔS (kJ/mol)	−396.24 ± 31.20
	ΔG (kJ/mol)	−40.61 ± 0.58
	K_a (M)	$1.2\pm0.2 \cdot 10^{7}$

** n value represents the molar ratio between streptavidin and biotinylated HA*

A complete thermodynamic analysis of biotin hydrazide-streptavidin binding was preliminary performed. A solution of streptavidin 6 µM in PBS 10 mM was titrated by stepwise injections of biotin hydrazide solution 100 µM in PBS 10 mM. Data were analysed with an independent site model, where the macromolecule has *n* independent and equivalent binding sites for a ligand.[3] Figure S.5 shows the experimental data obtained subtracting the heat of ligand dilution into the buffer.

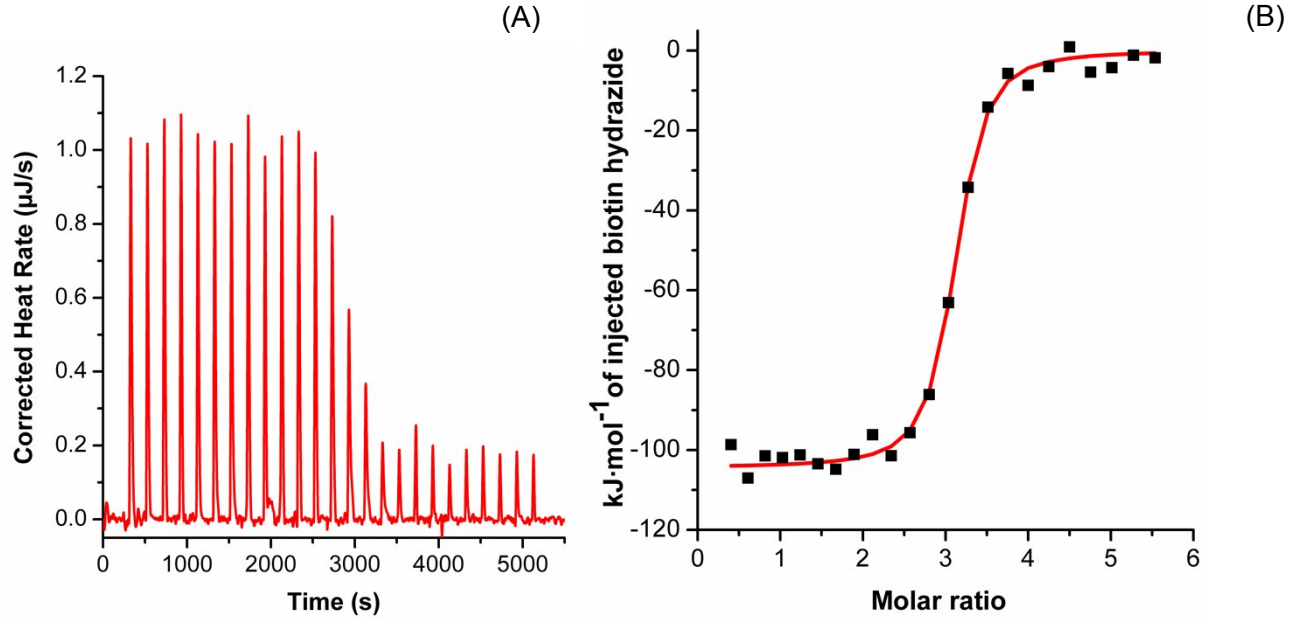

Figure S.5: *ITC data for titration by stepwise injection of biotin hydrazide 100 µM in PBS 10 mM, in a solution of streptavidin 6 µM in PBS 10 mM at 25 °C. The solid squares are the experimental data obtained by integrating the raw heat data and subtracting the heat of ligand dilution into the buffer. The lines represent the best fit obtained with the independent-sites model.*

Table S.4: *Thermodynamic parameters of the interactions between biotin hydrazide and streptavidin. The values represent the average deviation of different ITC measurements.*

Model	Variable	Value
Indipendent	K_d (M)	$7.23 \cdot 10^{-8} \pm 8.4 \cdot 10^{-8}$
	n	2.80 ± 0.51
	ΔH (kJ/mol)	−126.60 ± 27.86
	TΔS (kJ/mol)	−84.44 ± 31.96
	ΔG (kJ/mol)	−42.16 ± 4.10
	K_a (M)	$4.27 \cdot 10^{7} \pm 4.96 \cdot 10^{7}$

Thermodynamic parameters are reported in Table S.4. The interaction was enthalpy driven (ΔH=−126.60 kJ/mol) with a substantial entropy cost (ΔS=−84.44 kJ/mol) to achieve the net negative free energy change (ΔG=−42.16 kJ/mol). Even though we used the biotin hydrazide, the affinity to streptavidin is very high; in fact K_d ($K_d=1/K_a$) values are in the order of nM, in accordance with literature data.[4] These results are also in accordance with the thermodynamic characterization of biotin-streptavidin by ITC analysis reported by Wen-Yih Chen *et al.* (ΔG= −68.6 kJ/mol; ΔH= −133.8 kJ/mol; TΔS= −65.3 kJ/mol; n= 2.5).[5]
Little discrepancies can be probably ascribed to the terminal amine of biotin hydrazide molecules, used in our case, which could affect the binding with the streptavidin. This analysis has been used as reference point to next ones.
To establish the optimum range of concentrations to observe saturation, we titrated a solution of biotinylated hyaluronic acid, loaded into the cell, with streptavidin. We investigated a wide range of concentrations obtaining the best curve when 0.05 wt% Biot–HA was titrated with 16 µM streptavidin. The experimental data are shown in Figure S.6.

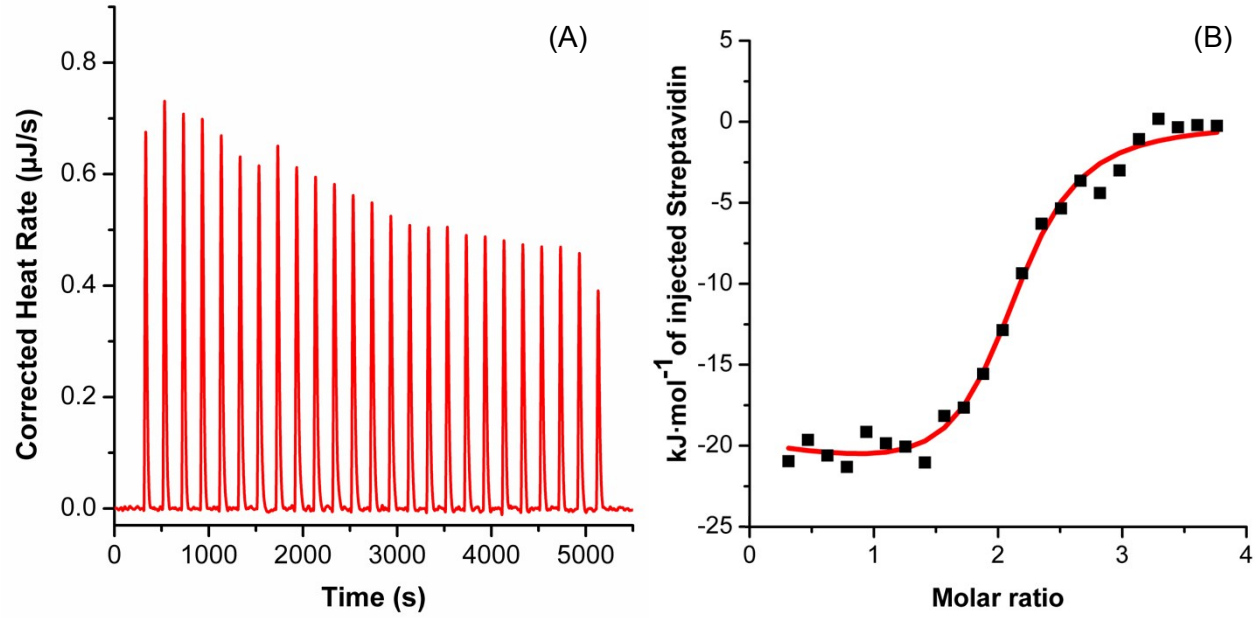

Figure S.6: *ITC data for titration by stepwise injection of streptavidin in a solution of HA-biotin 0.05 wt% at 25 °C. The solid squares are the experimental data obtained by integrating the raw heat data and subtracting the heat of ligand dilution into the buffer. The lines represent the best fit obtained with the independent-sites model.*

Table S.5: *Thermodynamic parameters of the interactions between biotinylated hyaluronic acid and streptavidin. The values represent the average deviation of different ITC measurements.*

Model	Variable	Value
Indipendent	K_d (M)	$1.81 \cdot 10^{-7} \pm 1.8 \cdot 10^{-7}$
	*n**	1.78 ± 0.15
	ΔH (kJ/mol)	−231.4 ± 84.15
	TΔS (kJ/mol)	−192.08 ± 87.22
	ΔG (kJ/mol)	−39.32 ± 3.08
	K_a (M)	$1.10 \cdot 10^{7} \pm 1.09 \cdot 10^{7}$

** n value represents the molar ratio between streptavidin and biotinylated HA*

The fitting parameters together with the calculated Gibbs free energy and the entropy gain are given in Table S.5. Although the binding process is exothermic (ΔH < 0), there is a considerable unfavourable entropic contribution probably due to the rearrangement of water molecules that play an important role in glycosaminoglycans (i.e HA).[6] Respect to previous experiment, in this case the high affinity between the biotinylated polymer and streptavidin was kept but the K_a value was slightly decreased ($K_a = 1.10 \cdot 10^7$ M). Because the biotin molecules were covalently linked to the polymer chain, a reduction of their degrees of freedom could be observed.
Biotin-streptavidin specific interaction was confirmed by HA titration with streptavidin. Raw data in Figure S.7 shows only small peaks of dilution, demonstrating that the streptavidin and HA do not interact.

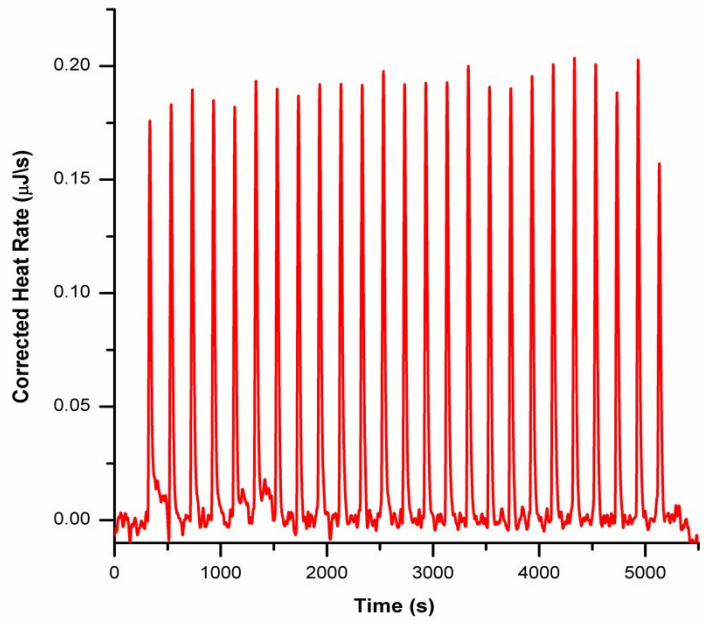

Figure S.7: *ITC data for titration by stepwise injection of streptavidin into 0.05 wt% HA at 25 °C.*

Nanocapsule decoration

A decoration strategy underlies the development of NCs in this study. ITC results were of fundamental importance to perform NCs assembly and avoid nonspecific interactions due to the addition of a larger amount of the biomolecules compared to site availability. A qualitative study of the specific interaction of streptavidin to biotinylated NCs was performed by confocal analysis. In accordance with ITC results, streptavidin, labelled with Atto 655, was added under sonication at a ratio 1:1 with the biotin to biotinylated and non-biotinylated O/W NEs. As shown in Figure S.8, the fluorescence intensity of the Atto-655-streptavidin was about 86.1% higher for biotinylated system when compared to non-biotinylated one, as consequence of the specific interaction with biotin-HA. No specific fluorescence signals were observed for the samples without biotin moieties. Analyses were performed on at least 3 images for each system.

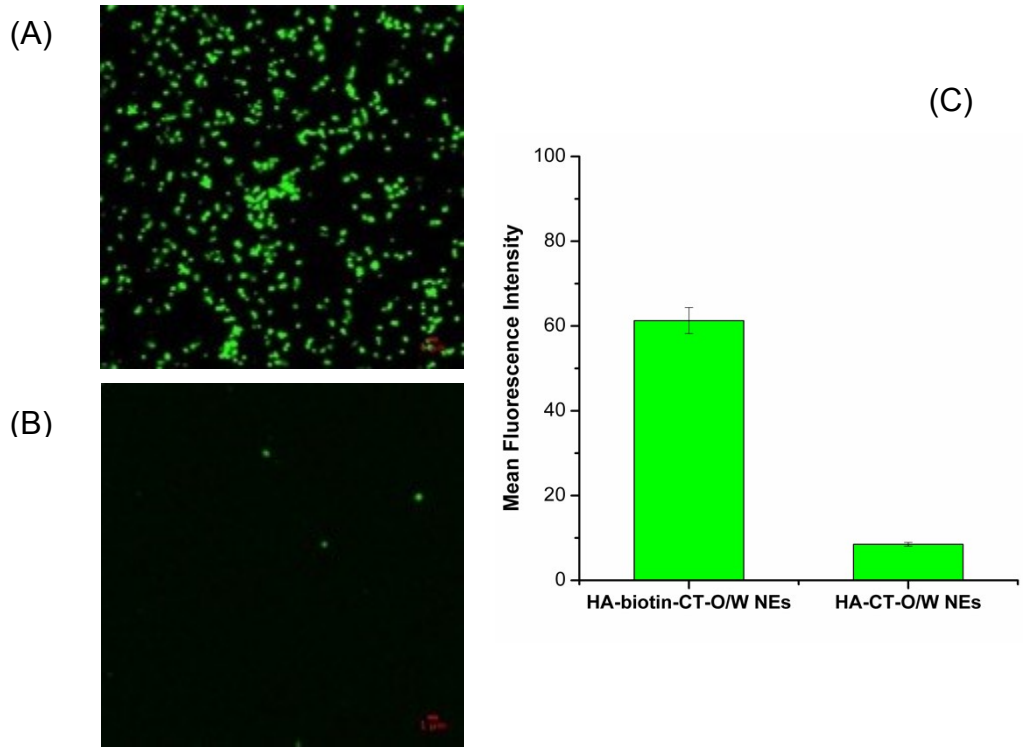

Figure S.8: *Confocal images of Atto 655-streptavidin interaction with HA-biotin-CT-O/W NEs (A) and HA-CT-O/W NEs (B) (scale bar is 1 μm). Plot of mean fluorescence intensity of Atto-655 labelled streptavidin(C). Data are reported as mean ± SD (n=3).*

Synthesis, purification and characterization of 5-FAM-CD44BP-WL

A 13-mer peptide that recognizes CD44 receptor has been previously identified. The amino acid sequence reported was: RLVSYNGIIFFLK (CD44BP without CGGG- linker CD44BP-WL). A coupling with 5-carboxyfluorescein (5-FAM) was performed to label the peptide at the N-term

(5-FAM-CD44BP-WL). Another non-α-amino acid (β-alanine) was introduced at the N-tem before the coupling reaction with 5-FAM to avoid an Edman-type elimination reaction.[7] Peptide synthesis was performed by exploiting the solid-phase peptide strategy (SPPS), using 9-fluorenylmethoxycarbonyl (Fmoc) chemistry and a super acid labile resin. 5-FAM-CD44BP-WL was synthetized and the resulting peptide was deprotected and cleaved from the resin. The crude peptide purity was assessed by analytical RP-HPLC, using a C-18 column with a linear elution gradient. The HPLC chromatograms of the crude and purified peptide chain are reported in Figure S.9. Unambiguous identification of the product at R_t = 27.44 min was accomplished through ESI-MS analysis whose mass spectrum is reported in Figure S.10.

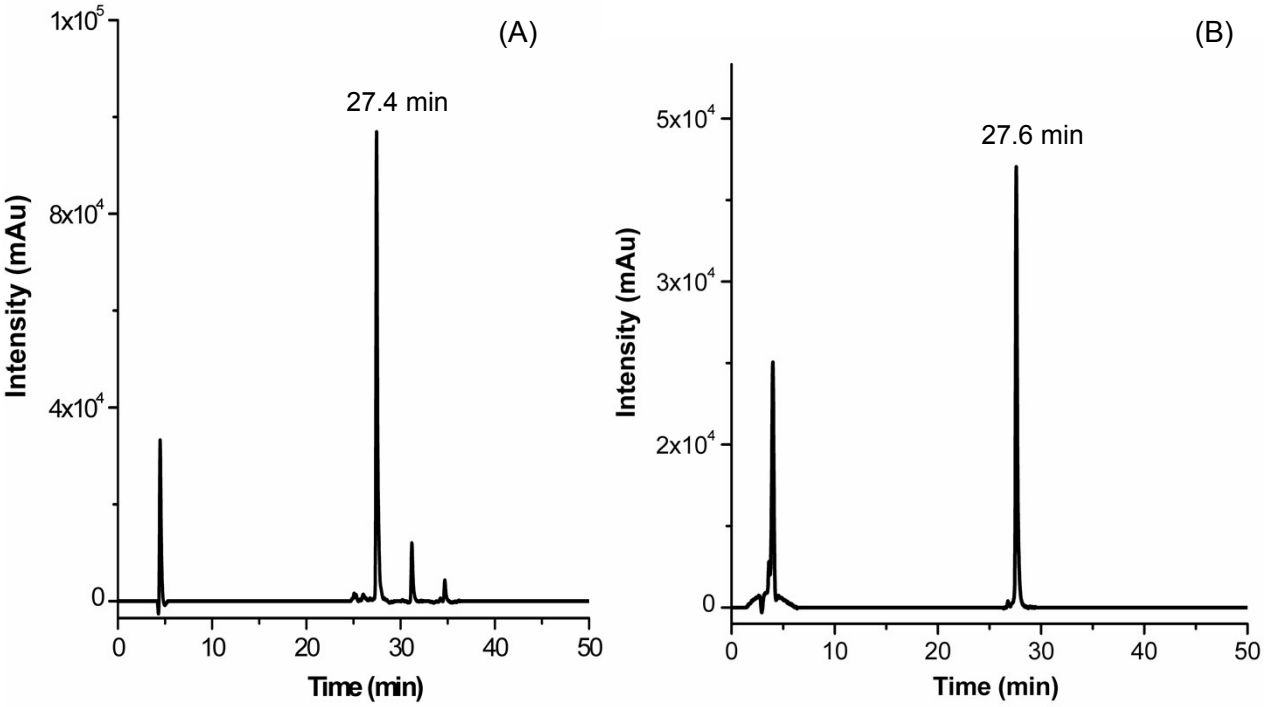

Figure S.9: *Analytical RP-HPLC of 5-FAM-CD44BP-WL crude peptide (A) and purified one (B). The chromatogram were detected at λ = 220 nm.*

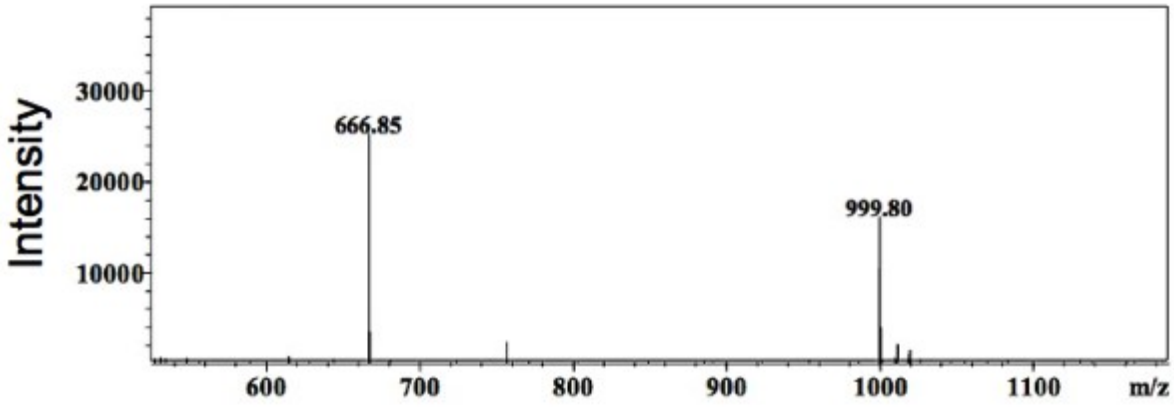

Figure S.10: *ESI-MS of the peak at R_t = 27.44 min. The two masses at m/z 666.85 and 999.80 represent respectively $[M+3H]^{3+}$ and $[M+2H]^{2+}$ of theoretical expected mass 1997.01 Da.*

The HPLC peak with R_t = 27.44 min was correlated to a mass peak of *m/z* 666.85 ($[M+3H]^{3+}$) and *m/z* 999.80 ($[M+2H]^{2+}$) which were consistent with the theoretical expected isotopic mass of 1997.01 Da of the peptide (observed mass: 1997.55 ± 0.5 Da).

Once the synthesis was completed, a small amount of product was analyzed by TANDEM mass spectrometry coupled to liquid chromatography. A single peak, corresponding to the desired peptide, was found and its product ion scan showed the expected fragmentations (Figure S.11 and Table S.6).

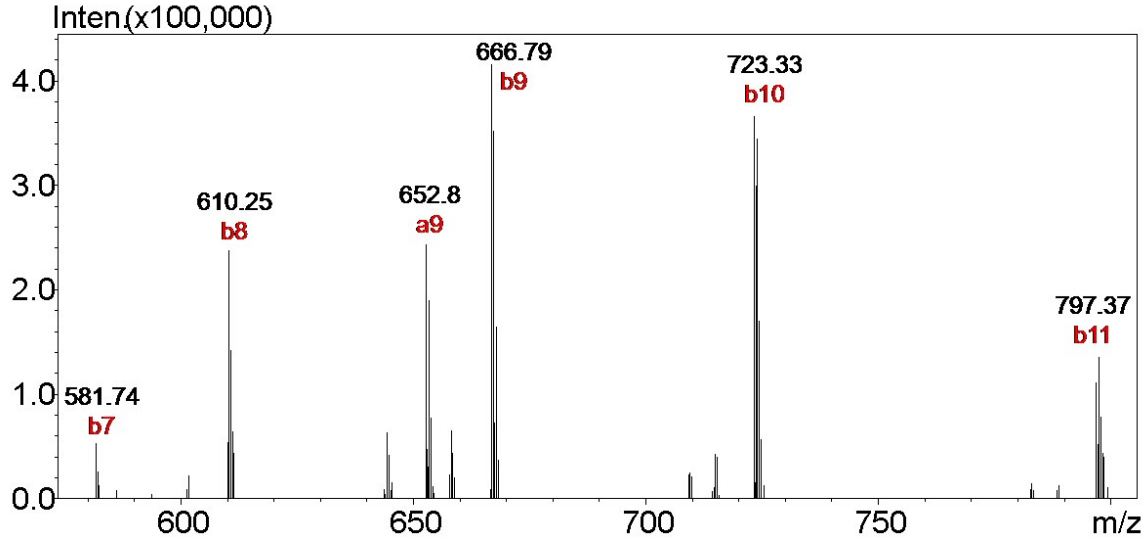

Figure S.11: *ESI-MS-MS fragmentation spectra of 5-FAM-CD44BP-WL.*

Table S.6: *Mass table of 5-FAM-CD44BP-WL fragmentations. Numbers in cyan represent the theoretical fragments identified in the experimental spectrum.*

#	b	b++	b+++	c	Sequence	y	y++	y+++	#
1					5FAM-βAla	1997.01	999.01	666.34	14
2	585.19			602.21	Arg	1568.93	784.97	523.65	13
3	698.27			715.30	Leu	1412.83	706.92	471.62	12
4	797.34	399.17	266.45	814.36	Val	1299.74	650.38	433.92	11
5	884.37	442.69	295.46	901.4	Ser	1200.68	600.84	400.89	10
6	998.41	499.71	333.48	1015.44	Asn	1113.64	557.33	371.89	9
7	1161.48	581.24	387.83	1178.5	Tyr	999.60	500.30	333.87	8
8	1218.49	609.75	406.84	1235.52	Gly	836.54	418.77	279.52	7
9	1331.58	666.29	444.53	1348.61	Ile	779.52	390.26	260.51	6
10	1444.67	722.84	482.23	1461.69	Ile	666.43			5
11	1591.73	796.37	531.25	1608.76	Phe	553.35			4
12	1738.80	869.91	580.27	1755.83	Phe	406.28			3
13	1851.89	926.45	617.97	1868.91	Leu	259.21			2
14					Lys	146.13			1

Further, 5-FAM-CD44BP-WL was purified by preparative RP-HPLC to yield the pure product (Figure S.12). Pure 5-FAM-CD44BP-WL was obtained in ~30% yield from the crude peptide and its purity was ascertained by analytical RP-HPLC, with an excellent purity of the 98%.

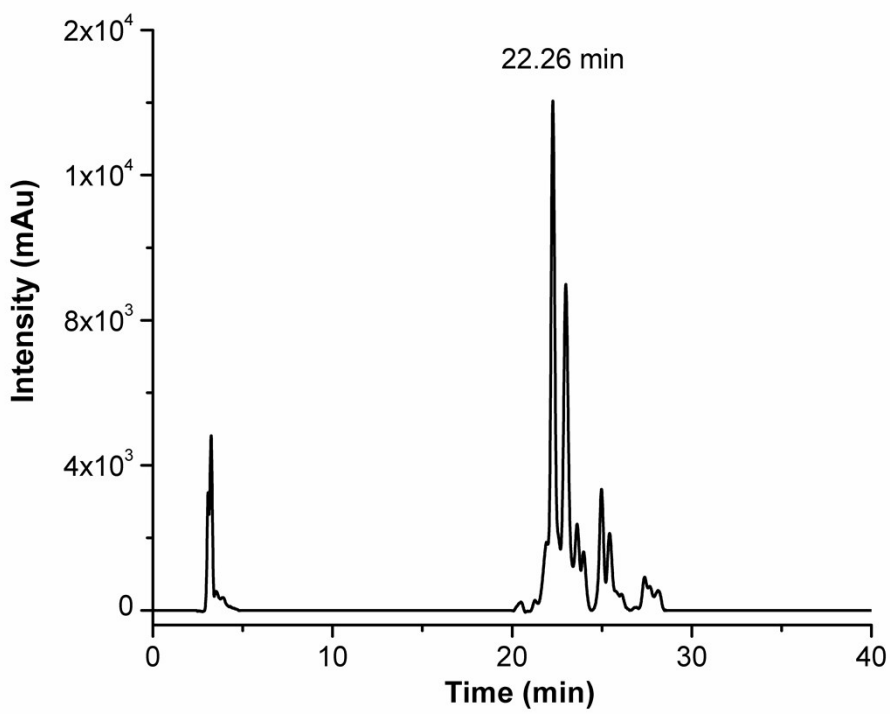

Figure S.12: *Preparative RP-HPLC chromatogram of the crude 5-FAM-CD44BP-WL peptide; the chromatogram was followed at λ = 220 nm.*

Cellular uptake of 5-FAM-CD44BP-WL

In order to verify the CD44BP-WL peptide recognition by CD44 receptor, cellular uptake experiments were performed. The binding and internalization of the CD44BP-WL into the cells were evaluated by confocal microscopy. Because it's widely reported that human primary glioblastoma cell line (U-87) over-expresses CD44 receptor, this cell line was chosen as positive control[8]. On the contrary, human umbilical vein endothelial cells (HUVECs) were considered as negative control due to their low CD44-expression[9]. Figure S.13 shows the normalized value of expression of CD44 in different cell lines as reported by Human Protein Atlans.[10] The over-expression of CD44 in the U-87 cells used for our experiments was also verified by real-time PCR analysis (Figure S.14).

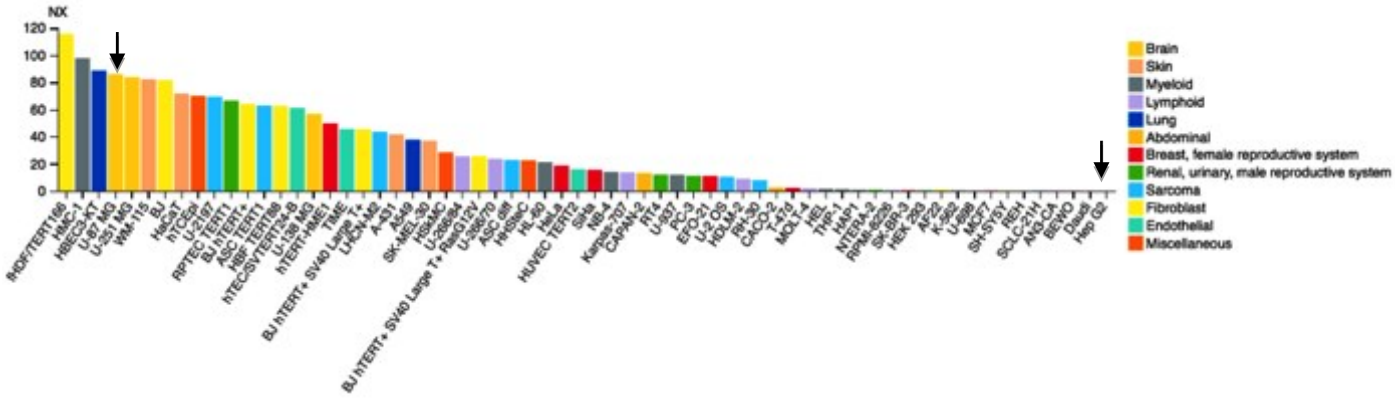

Figure S.13: *Cell lines ordered by descending CD44 expression. Black arrows indicates the position of U87 cells on the left and of HepG2 cells on the right. Image available at* www.proteinatlas.org.

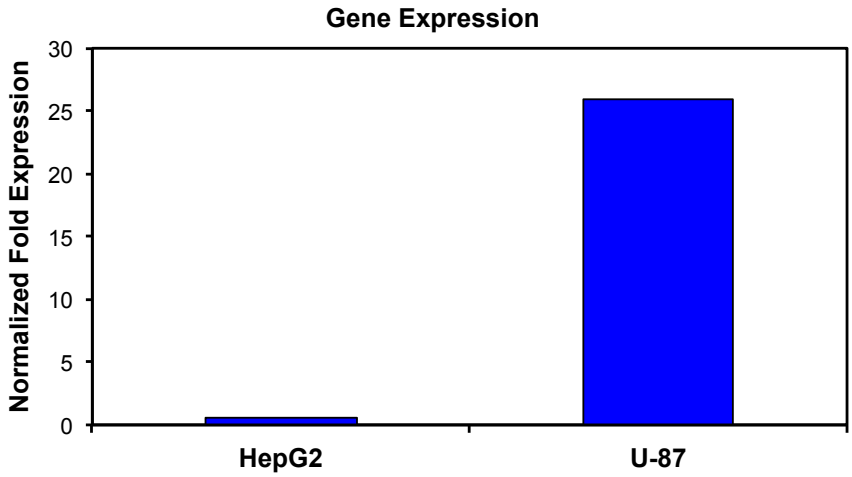

Figure S.14: *Real-time PCR analysis of CD44 expression for U-87 and HepG2 cell lines.*

U-87 human primary glioblastoma cells were grown in DMEM (10% FBS, 1% L-Glu, 1% Streptomycin penicillin) and human umbilical vein endothelial cells (HUVECs) were kept in M200 (20% FBS and supplemented with LGSG kit). After seeding, cells (2×10^5) were left 2 h to allow attachment. Then, they were incubated and treated with 5-FAM-CD44BP-WL dissolved in DMSO (final concentration in cells 8.5 μM), for 1 h in cell specific medium at 37°C. Cells were then washed twice with PBS and fixed for 20 min in 4% PFA. Nuclei and cell shape were labelled by DRAQ5 (excitation 633 nm) and Phalloidin 555 (labels cytoskeleton), respectively. The fluorescence intensity was analyzed by Zeiss LSM 710 confocal microscope. Images were reconstructed by ImageJ software.

Figure S.15 shows confocal microscopy images of a confluent monolayer of U-87 and HUVEC cells treated with 5-FAM-CD44BP-WL (8.75 μM) at 37 °C for 1 h under standard cell culture conditions. The peptide was completely internalized into glioblastoma cells as clearly results in the image obtained with an increased magnification. U-87 cells are positive to 5-FAM-CD44BP-WL internalization at a level of 87% more than HUVECs (Figure S.16). This can be ascribed to the specific peptide recognition by CD44-receptor over-expressed by tumor cells.

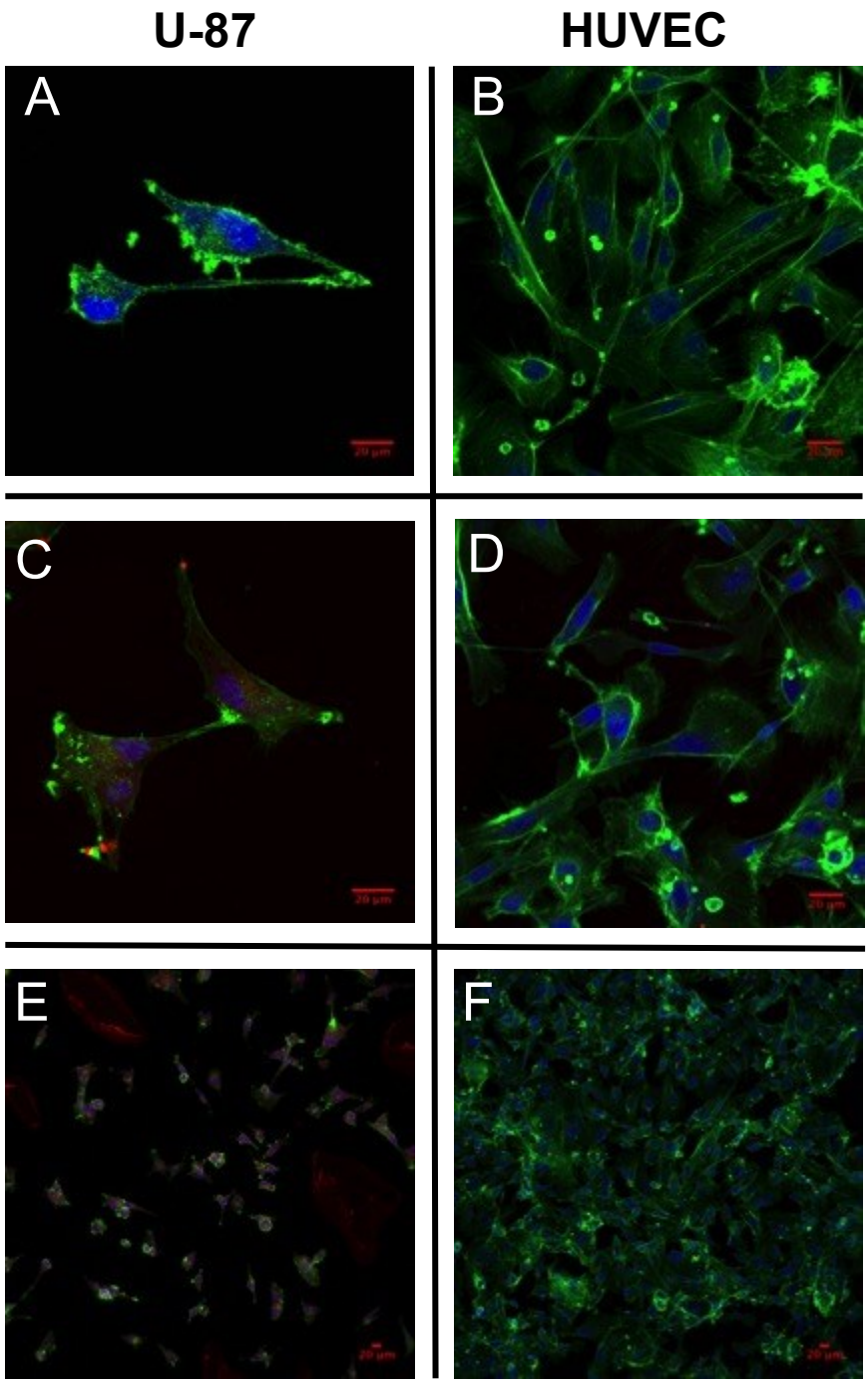

Figure S.15: *Confocal microscopy images showing 5-FAM-CD44BP-WL interactions with confluent monolayers of U-87 (C, E) and HUVEC (D, F) cells. For each cell line it is reported the image of untreated cells used as control (A, B). Nuclei (blue) and cytosol (green) of the cells were stained with DRAQ5 and Phalloidin 555 respectively, while red color represents peptide uptake. Scale bar was 20μm.*

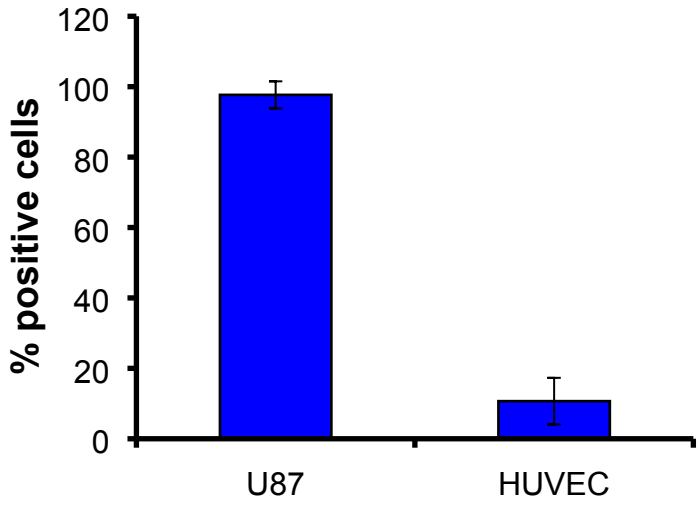

Figure S.16: *CD44BP-WL uptake in U87 and HUVEC cell lines. It is reported the number of positive cells to the peptide as mean ± SD (n=3).*

5-FAM-CD44BP-PEG$_{2k}$-biotin

Once confirmed 5-FAM-CD44BP-WL uptake, peptide sequence was modified as schematized in figure S.17; to allow the PEG conjugation at N-term.

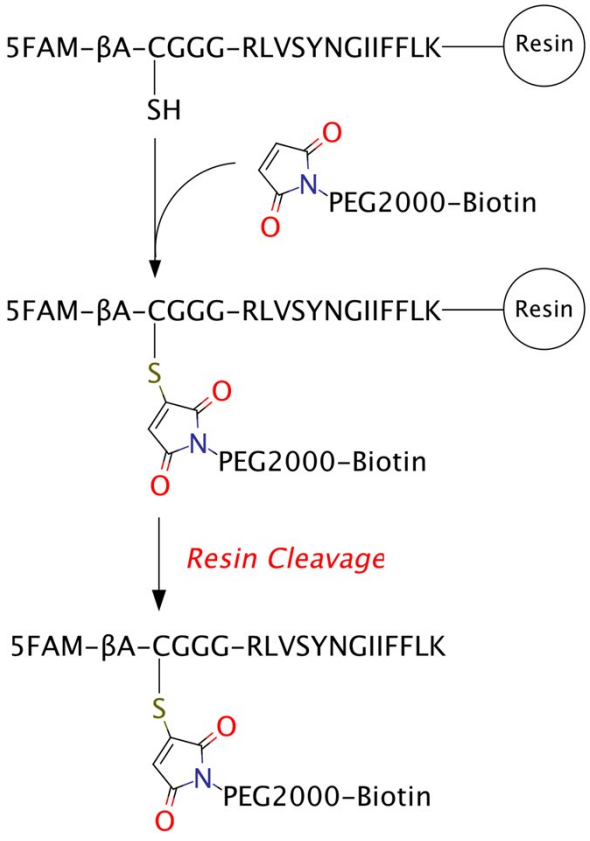

Figure S.17: *Schematic representation of the solid-phase synthetic strategy of PEGylated peptide.*

Figure S.18 shows ESI-MS spectrum of peptide sequence, before PEG conjugation (5-FAM-βA-CGGG-RLVSYNGIIFFLK)

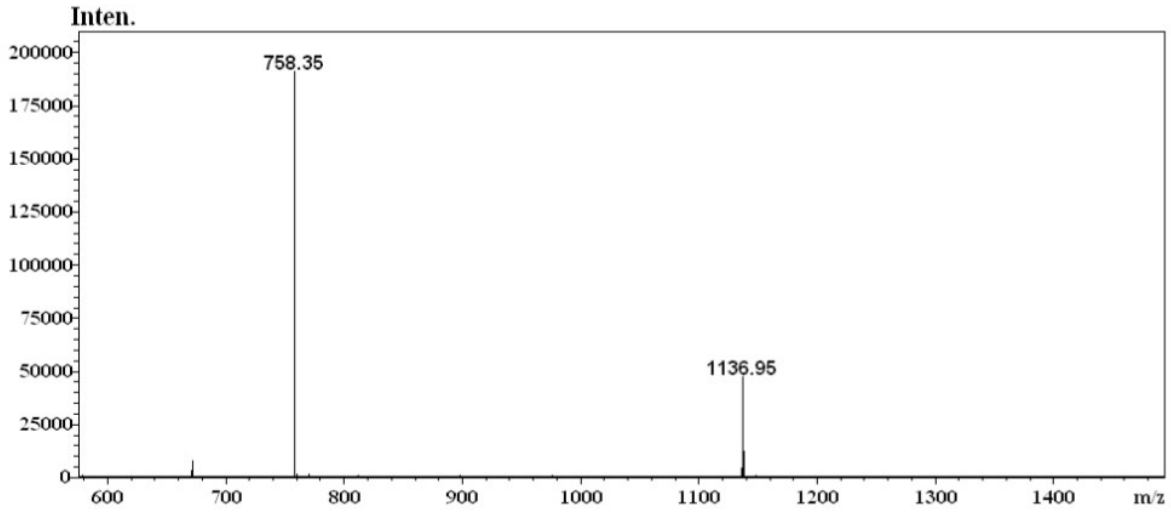

Figure S.18: *ESI-MS of 5-FAM-CD44BP. The two masses at m/z 758.35 and 1136.95 represent respectively* $[M+3H]^{3+}$ *and* $[M+2H]^{2+}$ *of theoretical expected mass 2271.08 Da.*

Once performed the coupling with the maleimide-PEG_{2k}-biotin linker, the peptide was deprotected and cleaved from the resin. The crude peptide purity was assessed by analytical RP-HPLC, using a C-18 column with a linear elution gradient. The crude biotin-PEG_{2k}-maleimide-peptide (5-FAM-CD44BP-PEG) was purified by preparative flash chromatography, using a Biotage ISOLERA flash purification system. The pooled fractions, containing the desired products, were analyzed by analytical RP-HPLC. In Figure S.19 are reported HPLC chromatograms of the crude and purified PEGylated peptide chain.

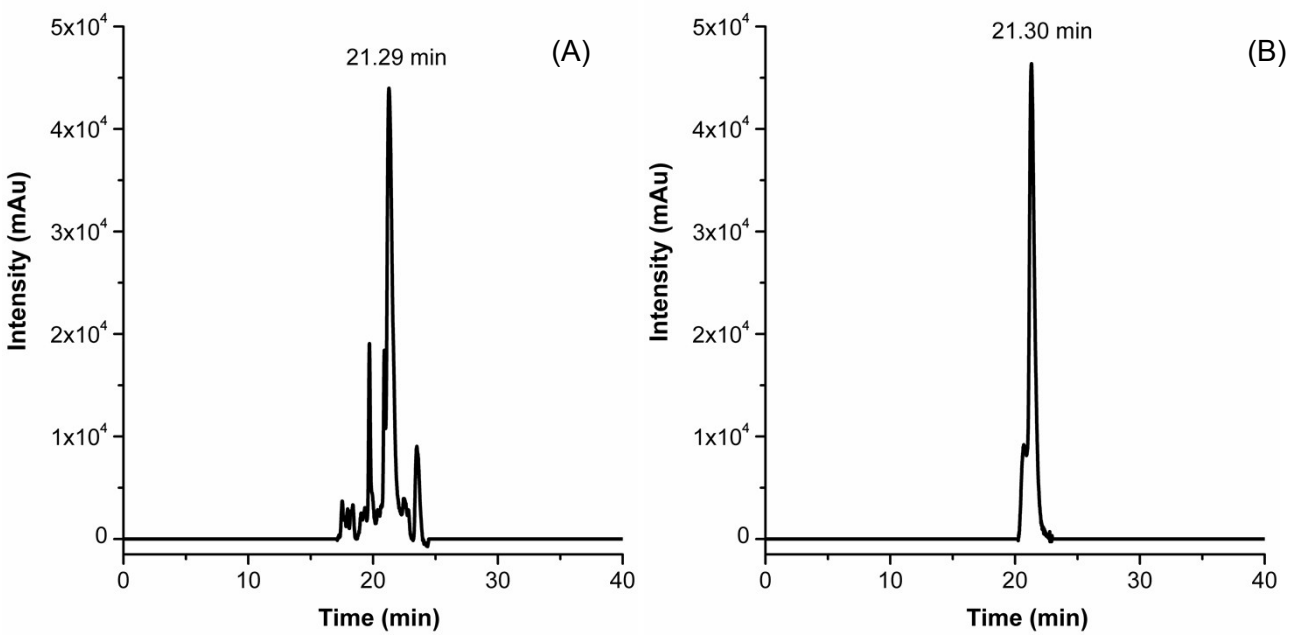

Figure S.19: *Analytical RP-HPLC of 5-FAM-CD44BP-PEG crude peptide (A) and purified one (B). The chromatogram were detected at λ = 220 nm.*

Matrix-assisted laser desorption/ionization time of flight (TOF) mass spectrometry

Figure S.20 show the MALDI mass spectra (centroid) of biotin-PEG_{2k}-Maleimide acquired before peptide conjugation. An intense, singly charged Gaussian distribution was observed with the most abundant ion at 2411.59 *m/z* and the typical expected ethylene oxide repeat unit of 44 Da, proving the presence of PEG within the sample. An increment of +23 *m/z* with respect to the expected mass was observed, which can be attributed to the sodiated species $(MNa)^+$. Because of the high affinity of PEG for both sodium and potassium, a cationization with Na^+ has been often observed.[11]

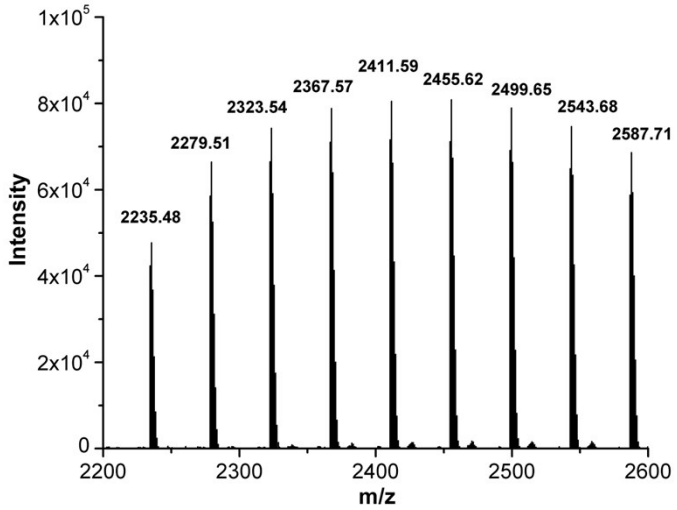

Figure S.20: *MALDI mass spectra (centroid) of Biotin-PEG-Maleimide linker*

Streptavidin and 5-FAM-CD44BP-PEG colocalization analyses

Colocalization of streptavidin and CD44BP-PEG built around the O/W NE was evaluated by confocal microscopy to confirm the specific interaction between them. To this purpose, Atto-655 conjugated to streptavidin and 5-FAM to peptide were used as dyes. Such a pair of fluorophores possesses excitation and emission spectra far enough apart from each other to avoid any cross talk. A widely reported method to evaluate the extent of colocalization is a simple images overlay deriving from different channels[12]. In Figure S.21 the superimposition of the red channel for the streptavidin and the green one for the peptide is reported. The resulting yellow/orange colour shows colocalization between the green and red signals meaning the correct deposition of the peptide on the streptavidin.

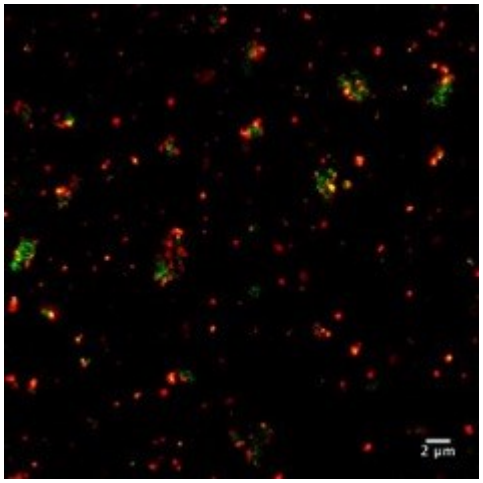

Figure S.21: *Overlay of confocal images of the Atto streptavidin-655 (red) and 5-FAM-CD44BP-PEG (green) built above the O/W NEs. Scale bar is 2 µm.*

In vitro cytotoxicity analysis

To investigate the behaviour of peptide functionalized NCs toward cancer cell lines, biological analyses were carried out. The oil core of the O/W NEs was pre-loaded with curcumin, which is a hydrophobic natural agent whose anticancer effects has already been demonstrated in different cancer cell lines, including U-87. In order to understand the appropriate incubation time to appreciate curcumin anti-tumor effect, a confluent monolayer of U-87 cells was incubated with curcumin loaded CD44BP-PEG-O/W NEs, diluted 1:5 in cell suspension, at a final curcumin concentration of 62.8 µM for several time points (30 min, 1 h, 2 h and 4 h). Moreover, cells were treated with standard cell medium alone as positive control and with free curcumin as negative control. After incubation, cells were washed and a quantitative evaluation of cell viability (normalized to positive control, which is set to 100%) was obtained by PrestoBlue assay after 24 h.

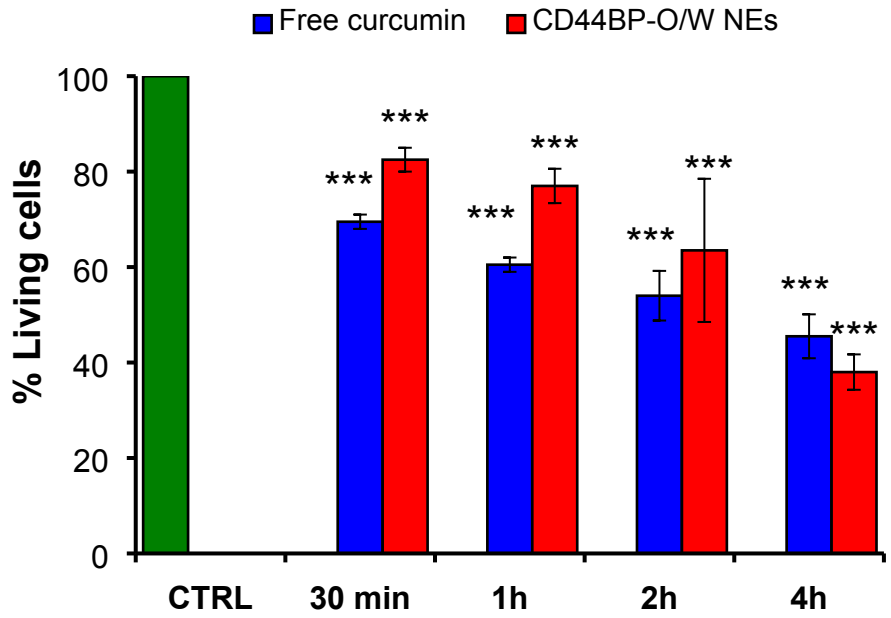

Figure S.22: *Cytotoxicity assay of curcumin loaded CD44BP-PEG-O/W NEs and free curcumin. U-87 cells were treated for several timepoints of incubation and cell viability was evaluated after 24 h. Data are reported as mean of three independent experiment ± SD (n=3) and expressed as percentage compared to control cells. The asterisk (***) indicates the statistical significance vs CTRL using Student's t test considering p ≤ 0.001.*

Data show an increase of cell mortality both for free curcumin and for CD44BP-PEG-O/W NEs over time. Indeed, curcumin significantly inhibited the vitality of U-87 cells in a dose and time dependent manner as largely reported.[13,14] At incubation times below 4 h free curcumin was more active than the encapsulated one most probably due to a partial internalization of the curcumin loaded nanocarrier (Figure S.22). Therefore, an incubation time of 4 h was selected for the successive experiment. Afterwards, control experiments were carried out treating cells with the un-functionalized NCs. A confluent monolayer of U-87 cells were incubated with curcumin loaded CD44BP-PEG-O/W NEs and PEG-O/W NEs, diluted 1:5 in cells, at a final curcumin concentration of 62.8 μM for 4 h for both of them. PEG-O/W NEs was used as negative control because it was assembled with the same streptavidin-biotin strategy described before, exhibiting a layer of PEG on the external nanocarrier shell (the same used for peptide PEGylation), without the targeting conjugated moieties. Moreover, cells were treated with cell medium alone as positive control and with free curcumin as second negative control. After incubation, cells were washed and a quantitative evaluation of cell viability (normalized to positive control, which is set to 100%) was performed after 24 h (Figure S.23).
Data showed a significant cytotoxicity effect of CD44BP-PEG-O/W NEs compared to blank. This is an evident consequence of peptide capability to accumulate the nanocarrier on the cells, thanks to ligand-receptor recognition, and to allow its internalization. CD44BP-PEG-O/W NEs exhibit an increase of 40% of cell death respect to unfunctionalized NCs, and a little difference in comparison with free curcumin.

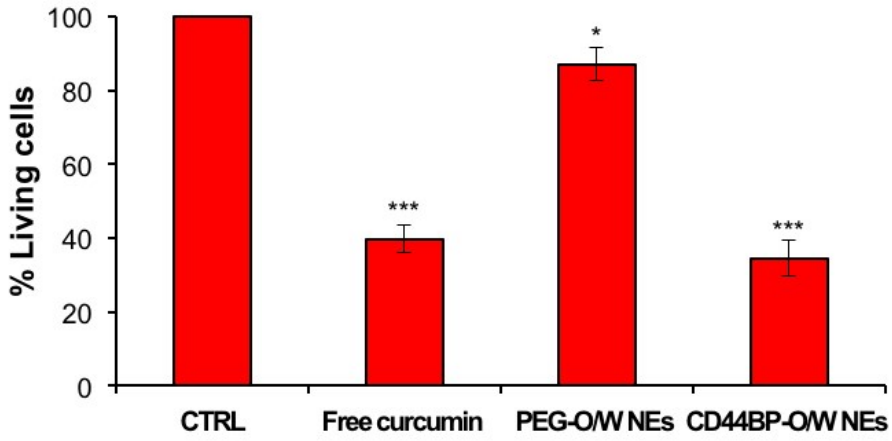

Figure S.23: *Cytotoxicity assay of curcumin loaded CD44BP- PEG-O/W NEs and PEG-O/W NEs, and free curcumin. U-87 cells were treated for 4h of incubation and cell viability was evaluated after 24 h. Data are reported as mean of three independent experiments ± SD (n=3) and expressed as percentage compared to control cells. The asterisk (*) indicates the statistical significance vs CTRL using Student's t test considering p <0.05; (***) p ≤ 0.001.*

Binding and uptake of CD44-targeted NCs by CD44-expressing cancer cells

A cellular uptake assay was performed by confocal microscopy to better investigate the cytotoxicity results and understand if the mortality observed could be attributed to curcumin. Curcumin has intrinsic fluorescence properties; therefore, it can be used as probe for NC detection. A confluent monolayer of U-87 cells were incubated with curcumin loaded CD44BP-PEG-O/W NEs and PEG-O/W NEs, for 4 h at the same experimental condition of cytotoxicity test described before. In addition, cells treated with cell medium alone were used as control (CTRL). Figure S.24 shows confocal microscopic images of U-87 cell monolayers after NC uptake, which strongly support the previous cytotoxicity results by showing strong fluorescence difference between CD44BP-PEG-O/W NEs and PEG-O/W NEs. However, no fluorescence can be detected from the images of the control cells (figure S.21 A, B). The presence of curcumin, displayed in red, in the cells cytoplasm as well as in the nuclei was clearly more evidenced for peptide functionalized NCs (90 ± 24 % more respect to the negative control). A possible explanation is that the peptide induces much higher internalization, in accordance with CD44BP uptake in U-87 cells described before. Furthermore, a slight amount of PEG-O/W NEs was detected in the cells. A probable justification could be attributed to passive internalization exerted by NCs especially those with diameters smaller than 200 nm, as ours are. In Figure S.25 is shown a plot of mean fluorescence intensity of curcumin encapsulated in CD44BP-PEG-O/W NEs and in PEG-O/W NEs normalized for the cell number. Data are expressed as mean of several images taken from at least three wells.

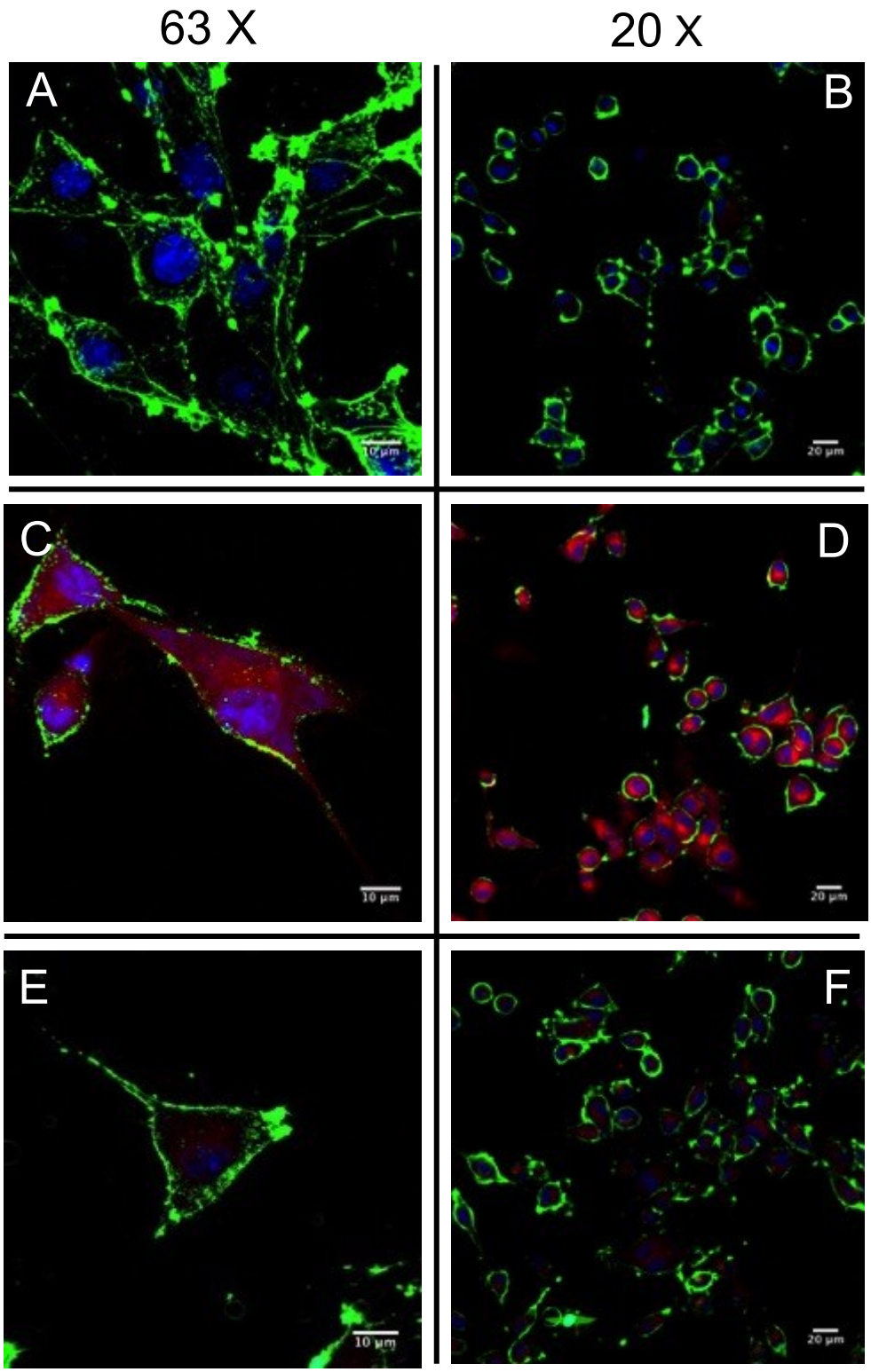

Figure S.24: *Confocal images of U-87 cells. (A, B) Untreated, (C, D) curcumin loaded C CD44BP-PEG-O/W NEs and (E, F) curcumin loaded PEG-O/W NEs interactions with a confluent monolayer of U-87 cells. Nuclei (blue) and cellular membrane (green) of the cells were stained with DAPI and WGA 555 respectively, while red color represents curcumin uptake. 63X and 20X refer to microscope objective. Scale bar is 10 µm for 63X images and 20 µm for 20X images.*

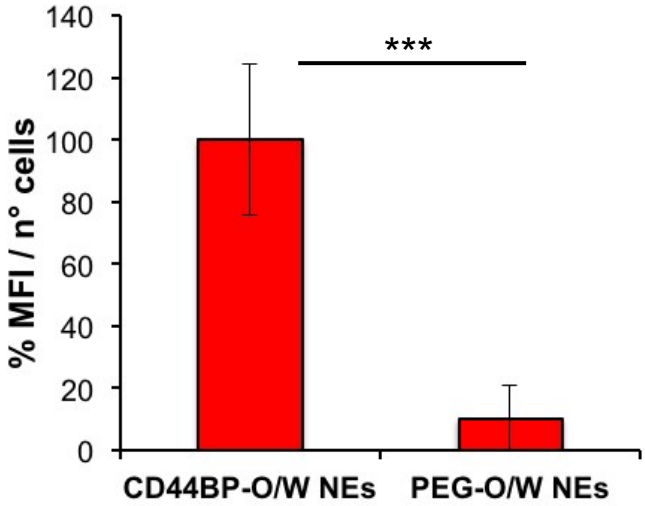

Figure S.25: *Plot of mean fluorescence intensity of curcumin normalized to cell number. U-87 cells were treated with curcumin loaded in CD44BP-PEG-O/W NEs and PEG-O/W NEs. Data are reported as mean ± SD (n=3).*

Cytotoxic test for U-87 cells of curcumin loaded and empty HA-coated O/W NEs is reported in Figure S.26. The carrier itself has been demonstrated to be safe.

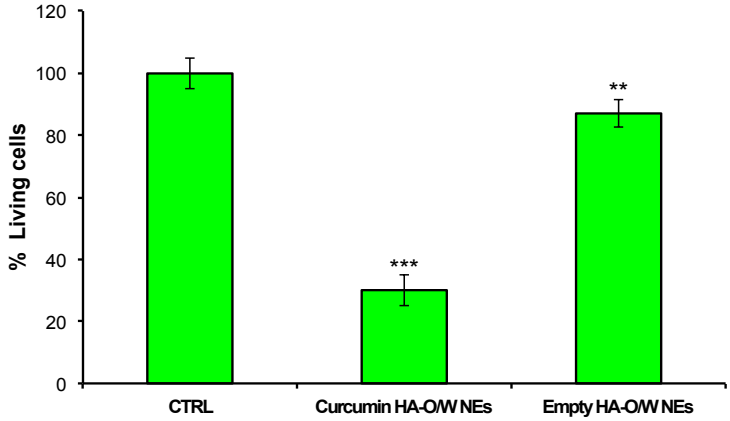

Figure S.26 *Cytotoxicity assay of curcumin loaded and empty HA-CT-O/W NEs. U-87 cells were treated for 4h of incubation and cell viability was evaluated after 24 h. Data are reported as mean of three independent experiments ± SD (n=3) and expressed as percentage compared to control cells. The asterisk (*) indicates the statistical significance vs CTRL, p ≤ 0.01 (**), p ≤ 0.001 (***).*

Figure S.27 shows plot of mean fluorescence intensity of curcumin normalized to cell number. HUVEC cells were treated with curcumin loaded in CD44BP-PEG-O/W NEs and PEG-O/W NEsconfocal microscopic images of HUVEC cell monolayers after NC uptake. The presence of curcumin appeared in red, while the cells cytoplasm and the nuclei were stained in green and blue respectively. Images are representative of at least three independent experiments, and ten images were examined for each treatment. HA-O/W NEs uptake was 89 ± 13 % higher than CD44BP-PEG-O/W NE one, while PEG-O/W NE uptake was not detected.

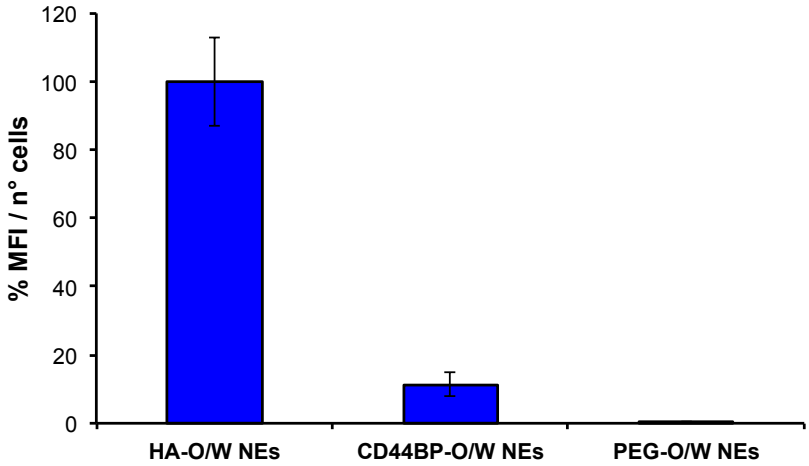

Figure S.27: *Plot of mean fluorescence intensity of curcumin normalized to cell number. HUVEC cells were treated with curcumin loaded in HA-CT-O/W NEs, CD44BP-PEG-O/W NEs and PEG-O/W NEs. Data are reported as mean ± SD (n=3).*

Bibliography

1. Vecchione, R. *et al.* Tunable stability of monodisperse secondary O/W nano-emulsions. *Nanoscale* **6**, 9300 (2014).

2. Mun, S., Decker, E. A. & McClements, D. J. Effect of molecular weight and degree of deacetylation of chitosan on the formation of oil-in-water emulsions stabilized by surfactant-chitosan membranes. *J. Colloid Interface Sci.* **296**, 581–590 (2006).

3. C. J. Martinez, et al., Isothermal Titration Calorimetry: Thermodynamic Analysis of the Binding Thermograms of Molecular Recognition Events by Using Equilibrium Models, in Applications of Calorimetry in a Wide Context – Differential Scanning Calorimetry, Isothermal Titration Calorimetry and Microcalorimetry, *InTech*, (2013).

4. Hyre, D. E. *et al.* Cooperative hydrogen bond interactions in the streptavidin-biotin system. *Protein Sci.* **15**, 459–467 (2006).

5. Kuo, T.-C., Tsai, C.-W., Lee, P.-C. & Chen, W.-Y. Revisiting the streptavidin-biotin binding by using an aptamer and displacement isothermal calorimetry titration. *J. Mol. Recognit.* **28**, 125–128 (2015).

6. Santos, H. A., Manzanares, J. A., Murtomäki, L. & Kontturi, K. Thermodynamic analysis of binding between drugs and glycosaminoglycans by isothermal titration calorimetry and fluorescence spectroscopy. *Eur. J. Pharm. Sci.* **32**, 105–114 (2007).

7. Bird, G. H., Crannell, W. C. & Walensky, L. D. Chemical synthesis of hydrocarbon-stapled peptides for protein interaction research and therapeutic targeting. *Curr. Protoc. Chem. Biol.* **3**, 99–117 (2011).

8. Lim, S. *et al.* Glioblastoma-secreted soluble CD44 activates tau pathology in the brain. *Exp. Mol. Med.* **50**, 1-11 (2018).

9. Dai, J. *et al.* Osteopontin induces angiogenesis through activation of PI3K/AKT and ERK1/2 in endothelial cells. *Oncogene* **28**(38), 3412–3422 (2009).

10. The Human Protein Atlas. Available at: https://www.proteinatlas.org

11. Bogan, M. J. & Agnes, G. R. Poly(ethylene glycol) Doubly and Singly Cationized by Different Alkali Metal Ions: Relative Cation Affinities and Cation-Dependent Resolution in a Quadrupole Ion Trap Mass Spectrometer, *J. Am. Soc. Mass Spectrom.,* **13**(2), 177-186 (2002).

12. Bolte, S. & Cordelières, F. P. A guided tour into subcellular colocalization analysis in light microscopy. *J. Microsc.,* **224**, 213–232 (2006).

13. Gersey, Z. C. *et al.* Curcumin decreases malignant characteristics of glioblastoma stem cells via induction of reactive oxygen species, *BMC Cancer,* **17**(1), 99 (2017)

14. Klinger, N.V., Mittal, S. Therapeutic Potential of Curcumin for the Treatment of Brain Tumors. *Oxid. Med. Cell Longev*., **2016**,9324085 (2016)